



ORIGINAL ARTICLE

Influential parameters in the shear strength of RC beams without stirrups

Parâmetros que influenciam na resistência ao cisalhamento de vigas de concreto armado sem estribos

Guilherme Frank Leme^a Elyson Andrew Pozo Liberati^b Marília Gonçalves Marques^c Leandro Mouta Trautwein^a Luiz Carlos de Almeida^a ^aUniversidade Estadual de Campinas – UNICAMP, Faculdade de Engenharia Civil, Arquitetura e Urbanismo, Campinas, SP, Brasil.^bUniversidade Estadual de Maringá – UEM, Departamento de Engenharia Civil, Maringá, PR, Brasil.^cUniversidade Federal de Viçosa – UFV, Rio Paranaíba, MG, Brasil.

Received 29 October 2021

Accepted 18 September 2022

Abstract: Experimental investigations have been commonly used to improve the existing knowledge about structural design, presenting accurate conclusions regarding structure behavior. However, considering the limitations of experimental studies, such as restricted amount of strain gauges, unexpected pathologies, difficulties to foresee the correct position of cracks, or simply saving in costs, the use of numerical analysis can present some innovative approaches to understand the process of failure in concrete elements, presenting easier results where experimental programs can hardly report. This study presents the numerical analysis of eight beams experimented by Sherwood [26], with two different sizes and variable aggregate sizes, seeking to understand the influence of coarse aggregate size in shear strength of beams without stirrups. The numerical approach was used to derive the influence of each internal shear mechanism and to identify the specific amount of dowel force, shear transfer by uncracked compression zone and aggregate interlock portion. The results showed that fair results can be obtained by 2D smeared crack approaches, enabling the identification of major aggregate interlock portion in beams with bigger coarse aggregate sizes. Comparing the size effect in beams allowed us to conclude that a higher contribution of aggregate interlock contribution can be obtained in large beams, with almost 64% of the total contribution, whereas smaller beams had only 43%. To evaluate the accuracy of the studied mechanisms, the results of Sherwood [26] were compared with the standards Model Code [23], CSA-A.23.3 [24], NBR 6118 [38], and ACI 318 [39]. Regarding the prediction of element rupture by concrete internal mechanisms, the normative instructions Model Code [23] and CSA A.23.3 [24] were the closest to the experimental results.

Keywords: reinforced concrete, shear, numerical analysis, beams.

Resumo: Investigações experimentais têm sido comumente usadas para melhorar o conhecimento existente sobre o projeto estrutural, apresentando conclusões precisas sobre o comportamento da estrutura. No entanto, considerando as limitações dos estudos experimentais, como quantidade restrita de extensômetros, patologias inesperadas, dificuldades de previsão do correto posicionamento das fissuras ou simples economia de custos, o uso da análise numérica pode apresentar algumas abordagens inovadoras para a compreensão do processo de falha em elementos de concreto, apresentando resultados mais fáceis onde programas experimentais dificilmente podem relatar. Este estudo apresenta a análise numérica de oito vigas experimentadas por Sherwood [26], com dois tamanhos diferentes e agregados de tamanhos variados, buscando-se entender a influência do tamanho do agregado na resistência ao cisalhamento de vigas sem estribos. A abordagem numérica foi usada para avaliar a influência de cada mecanismo de cisalhamento interno e para identificar a quantidade específica de força de pino, transferência de cisalhamento na zona de compressão não fissurada e a parcela de intertravamento de agregados. Os resultados mostraram que resultados razoáveis podem ser obtidos por abordagens de fissuras distribuídas 2D, permitindo a identificação da maior porção de intertravamento do agregado em vigas com maiores tamanhos de agregado graúdo. A comparação do efeito de escala em vigas permitiu

Corresponding author: Elyson Andrew Pozo Liberati. E-mail: eapliberati@uem.br

Financial support: None.

Conflict of interest: Nothing to declare.

Data Availability: The data that support the findings of this study are available from the corresponding author, [G.F. Leme].



This is an Open Access article distributed under the terms of the Creative Commons Attribution License, which permits unrestricted use, distribution, and reproduction in any medium, provided the original work is properly cited.

concluir que uma maior contribuição do intertravamento de agregados pode ser obtida em vigas grandes, com quase 64% da contribuição total, enquanto as vigas menores tiveram apenas 43%. Os resultados de Sherwood [26] foram comparados com as normas Model Code [23], CSA-A.23.3 [24], NBR 6118 [38] e ACI 318 [39] para avaliar a precisão das normas estudadas. Com relação a previsão da ruptura dos elementos por meio dos mecanismos internos do concreto, as instruções normativas Model Code [23] e CSA A.23.3 [24] resultaram valores mais precisos.

Palavras-chave: concreto armado, cisalhamento, análise numérica, vigas.

How to cite: G. F. Leme, E. A. P. Liberati, M. G. Marques, L. M. Trautwein, and L. C. Almeida, "Influential parameters in the shear strength of RC beams without stirrups," *Rev. IBRACON Estrut. Mater.*, vol. 16, no. 4, e16406, 2023, <https://doi.org/10.1590/S1983-41952023000400006>

1 INTRODUCTION

Several studies have attempted to understand the shear behavior of reinforced concrete (RC) beams, and various approaches to predict its strength have been proposed. Some important studies, primarily proposed by Ritter and Die Bauweise [1] and Mörsch [2], present the strength of concrete beams with stirrups as an analogy for a trussed system, wherein the steel and concrete stresses must be maintained under a factored capacity limit. This limit is considered as a function of the concrete and steel limits, assuming that only the stirrups resist the formation of cracks.

Without shear reinforcement, the strength mechanism of concrete typically relies solely on the nonlinear behavior of the concrete used, considering that the cracks can transmit normal and parallel forces to their formation site. These results in mechanical responses help avoid the failure of the structural element to a certain extent. Figure 1 shows the shear capacity mechanisms of reinforced concrete beams, where V_{cz} is the shear strength of the un-cracked concrete in the compression zone [3]; V_{agg} is the aggregate interlock interface shear transfer, also referred to as crack friction [4]–[10]; and V_{dowel} is the dowel action due to the longitudinal reinforcement bars [3], [11]–[16].

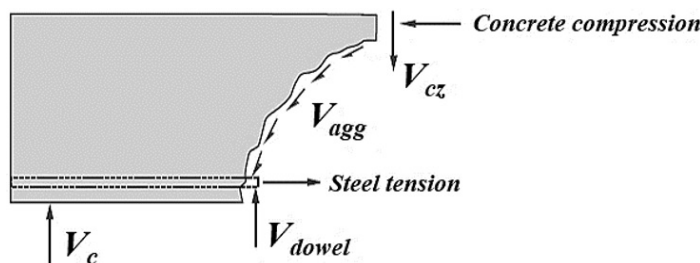


Figure 1. Shear transfer mechanism in RC beams.

Considering that the design codes are based on empirical equations, employing simple models - as the strut and tie models - on the structural members without transverse reinforcement results in an unsafe design. Bazant and Kazemi [17], Kani [18], and Taylor [19] tested beams based on empirical equations that are not applicable for practical situations.

Many studies have been conducted in the last 40 years on the internal capacity of concrete to resist shear strength, promotion owed to the continuing need to understand the real effect of these parameters on structural elements. To this end, several theoretical approaches have been proposed such as the modified compression field theory (MCFT) by Vecchio and Collins [20], and Bentz et al. [21], and the critical shear crack theory (CSCT), developed by Muttoni and Fernández Ruiz [22]. MCFT and CSCT consider the influence of aggregate size, size effect, and strain on RC shear capacity. These methodologies compose the basis of recent design codes, such as Model Code [23] and CSA-A23.3 [24].

In the 1970s, Walraven [25] presented an experimental method to understand the influence of aggregate interlock mechanism on shear strength and found that raising coarse aggregate size resulted in increased major shear strength. Paulay et al. [14] compared longitudinal bars of different diameters, crossing a discontinuous surface on an experimental block, allowing for an investigation on the influence of the dowel force on shear strength. The study related higher shear strengths to larger bar diameters acting like dowels.

Despite the importance of these studies, no clear conclusions can be drawn regarding the influence of each mechanism on the total shear strength of RC beams. Other experimental studies such as those conducted by Sherwood [26], Daluga et al. [27], and Yang and Ashour [28] found that the influence of the coarse aggregate size could result in an increased shear capacity. However, to obtain a clearer understanding of stress and strain distribution inside RC beams, numerical modeling tools are still necessary.

Belbachir et al. [29] conducted an experimental study on three sizes of geometrically similar concrete beams without transverse reinforcements. The shear span-to-depth ratio (a/d) was set to 2.5. For the beams tested with this ratio, the aggregate interlock mechanism was not completely activated at the failure load, especially for smaller beams. This shear transfer mechanism exhibits size dependence, which is primarily related to the crack shape.

To contribute to the understanding of the shear strength mechanism in beams without stirrups, this study presents a numerical non-linear modeling for eight beams experimentally tested by Sherwood [26].

This study is motivated by the need to develop numerical approaches to analyze structural elements using computational tools and understand the role of each internal shear capacity mechanism on the strength of RC beams without stirrups. Performing numerical simulation of the experimental cases typically involves two main phases: calibrating the model; and analyzing internal cracks, strains, and stress (typically limited to obtaining measurements from sensors or strain gauges).

This study aims to deepen the studies on the phenomena of shear strength of reinforced concrete beams without stirrups, regarding the internal mechanisms of the concrete to resist the shear force of beams, usually called V_c in technical standards.

In these design standards, V_c is usually used as a shear strength contribution portion and is considered in the determination of shear reinforcement. The greater the portion of shear strength force by internal mechanisms, the smaller the portion of shear force that an engineer, instructed by technical standards will calculate and apply as a form of transverse reinforcement ratio.

2 EXPERIMENTAL PROGRAM

To investigate the influence of each internal strength mechanism on the total shear strength, the first step was to find an experimental program capable of standardizing many parameters and allowing for comparisons between the several shear-influencing factors. Based on these requirements, Sherwood [26] reported different campaigns of RC beams without stirrups, using different sizes of coarse aggregate and other similar attributes as premises. These methods, paired with an effective registration of the principal parameters experimentally obtained, make the study a useful reference for numerical analysis.

Table 1 shows the main characteristics of the specimens used as reference for the numerical analysis, where b_w is the cross-section width, d the effective depth, L the effective beam length, d_{ag} the aggregate diameter, f_c the concrete compressive strength, and A_{s+} is the cross-section of longitudinal tensile reinforcement. The aggregate diameter was used as an input parameter as recommended by the Model Code [23], such as: tensile strength, elasticity modulus, and Poisson coefficient. Sherwood [26] considered two categories of beam sizes and types in the experiment: eight beams of size $122 \times 363 \times 1,800$ mm, called the *Small (S) Series* and, eight beams of size $295 \times 1,510 \times 9,000$ mm, called the *Large (L) Series*. Figure 2 shows the characteristics of the beams analyzed in this study. The samples possess different concrete strengths. Four different sizes of coarse aggregate are used, with the major aggregate size varying from 9.5 mm to 51 mm. The specimens were not reinforced with stirrups and all experiments were loaded until shear failure.

Reinforcement yield stresses were experimentally evaluated and recorded. Table 2 shows the yield values and nominal areas.

Table 1. Experimental Series.

Series	b_w [mm]	d [mm]	L [mm]	d_{ag} [mm]	f_c [MPa]	A_{s+} [mm ²]
<i>S-Series</i>						
S-10N1	122	280	1,620	9.5	41.9	285.2
S-10N2	122	280	1,620	9.5	41.9	285.2
S-20N1	122	280	1,620	19	39.2	285.2
S-20N2	122	280	1,620	19	38.1	285.2
S-40N1	122	280	1,620	38	29.1	285.2
S-40N2	122	280	1,620	38	29.1	285.2
S-50N1	122	280	1,620	51	43.5	285.2
S-50N2	122	280	1,620	51	43.5	285.2
<i>L-Series</i>						
L-10N1	300	1,400	8,100	9.5	38.4	3,500.0
L-10N2	300	1,400	8,100	9.5	40.4	3,500.0
L-20N1	300	1,400	8,100	19	31.4	3,500.0
L-20N2	300	1,400	8,100	19	33.2	3,500.0
L-40N1	300	1,400	8,100	38	28.1	3,500.0
L-40N2	300	1,400	8,100	38	28.5	3,500.0
L-50N1	300	1,400	8,100	51	41.0	3,500.0
L-50N2	300	1,400	8,100	51	40.1	3,500.0

S, and L – Smaller or larger specimen; 10, 20, 40, and 50 – Nominal aggregate sizes used in the test; N – Normal concrete compressive strength; 1, and 2 – Specimen 1 or 2 of the duplicated series.

Table 2. Experimental data on the steel bars used in the tests by Sherwood [26]. Where, f_y is the yield strength of reinforcement.

Bar type	Diameter [mm]	Area [mm ²]	f_y [MPa]
#3	10	71.3	494
20M	20	300	484
30M	30	700	452

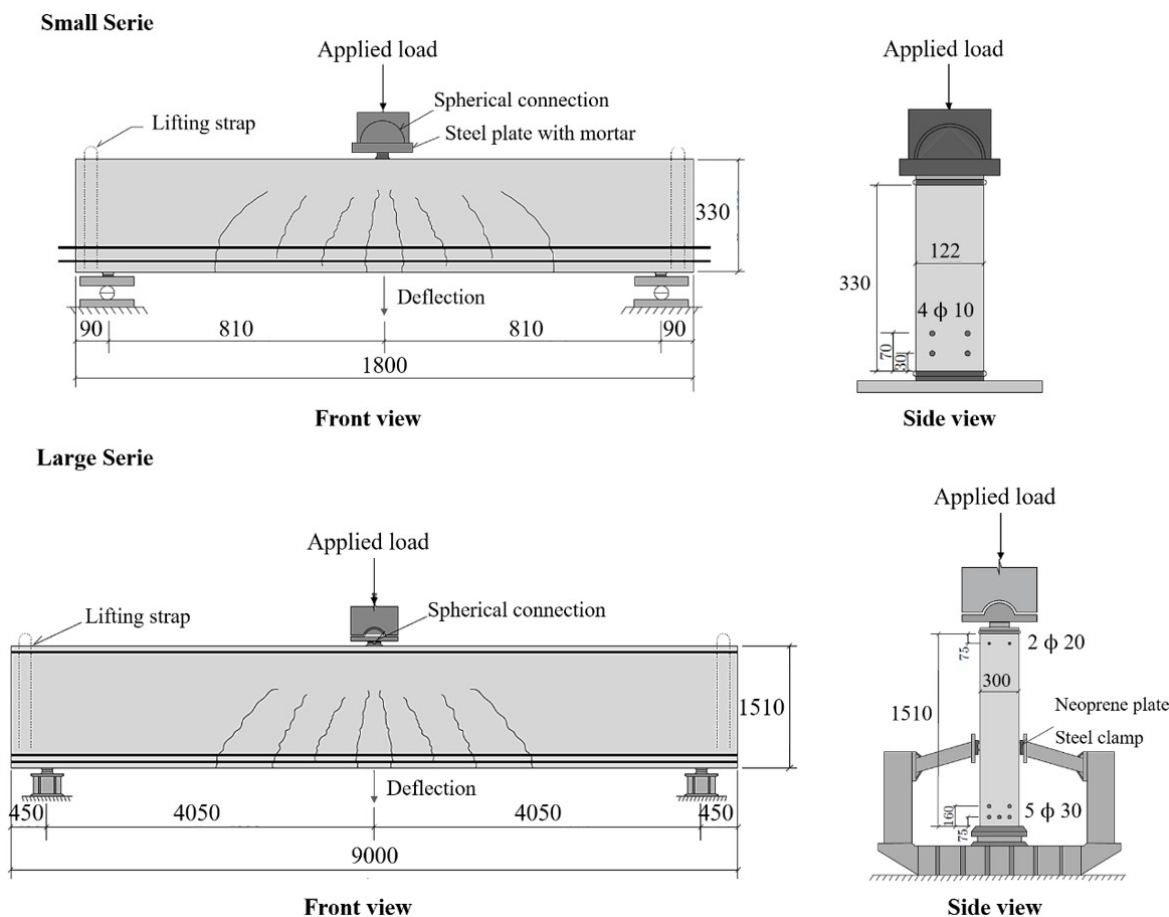


Figure 2. Beams of S-Series and L-Series of the experimental program (units in mm). Adapted by Sherwood [26].

3 NUMERICAL MODELS

A numerical model was developed to accurately simulate the experimental program. The problem was split into several partial problems and determined the internal relationship based their contour connectivity and characteristics. This is called the finite-element method (FEM). The FEM model must consider many effects to model the RC beams correctly and derive the basic conditions for the interaction between steel and concrete and the gradual formation of cracks.

The models tested in the laboratory were reproduced using DIANA 10.1. The discretization of the mesh in the S- Series used quadratic finite elements of approximately 26×26 mm, which is approximately $1/12$ of the total beam height (330 mm), which has been by Feenstra et al. [30], Vecchio and Shim [31], and Pimentel et al. [32]. In the L- Series, the mesh proportion contained quadratic finite elements of approximately 75×75 mm, on the order of $1/20$ of the total beam height (1,510 mm). Figure 3 shows the boundary conditions, load application points, and mesh sizes used in the FEM simulations.

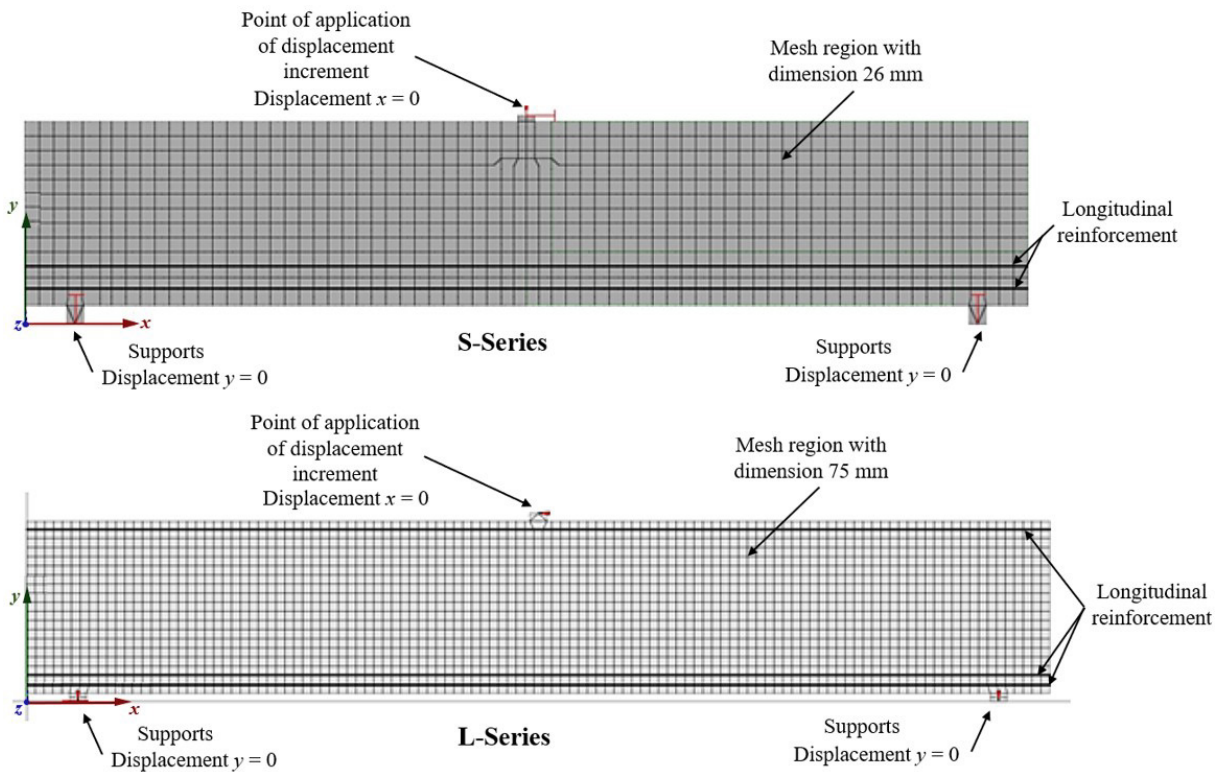


Figure 3. S and L series beams numerical model.

The models were constructed with 2D plane stress elements using square and triangular formats to represent the exact position of loads, restrictions, and longitudinal reinforcements. The longitudinal bars employ stiff beam elements for longitudinal and transverse displacements, particularly to act as dowels when the crack occur near the reinforcement.

The beams were configured to present two vertical restrictions at the supports, in addition to the horizontal restriction at the load point. The load was applied with a continuous displacement of 0.05 mm during each load step. The modified Newton-Raphson method was used to reach the convergence, with an internal energy-based criterion and a tolerance of 0.001. To accelerate the convergence, the line search and arc-length method were included in the model, according to the recommendations described in DIANA [33].

Table 3 shows the main parameters used to simulate the concrete and steel materials used in this study. These parameters were obtained with numerous analyses, aiming to ensure consistency between numerical models and the experimental program. The data obtained by Sheerwood [26] were used as values for f_c , the other properties were obtained based on the Model Code [23] recommendations, such as tensile strength of concrete, (f_{ct}), elasticity modulus of concrete (E_c), and concrete Poisson coefficient (ν). Based on these values, calibrations were performed for each parameter and the ideal calibrated model was chosen.

The evaluation included 4 to 5 energy ranges from fracture to traction. The initial value was adopted as recommended by the CEB/FIP Model Code [34] with a maximum reduction of 40% for L-Series beams and up to 30% for S-Series beams.

Based on the parametric analysis performed, for the models studied, the increase in fracture energy proportionally reduced the load capacity of the analyzed beams, presenting reductions of 30-40% of the fracture energy in traction to better approach the experimental result. According to the CEB/FIP Model Code [34], the fracture energy can be estimated from Equation 1, which depends on the fracture energy base value, as shown in Table 4.

$$G_f = G_{F0} \left(\frac{f_c}{10} \right)^{0.7} \tag{1}$$

Table 3. Parametrization of concrete and steel at beams type S- and L-Series. Where: Exp.⁽¹⁾ refers to Exponential Tensile Softening.

Specimen	S-10	S-20	S-40	S-50	L-10	L-20	L-40	L-50
d_{ag} [mm]	9.5	19	38	51	9.5	19	38	51
f_c [N/mm ²]	41.9	38.1	29.1	43.5	38.4	31.4	28.1	40.1
f_{ct} [N/mm ²]	2.5	2.4	2.1	2.3	2.35	1.96	1.94	2.20
E_c [N/mm ²]	27,215	25,450	25,717	27,482	25,000	23,000	23,674	25,000
ν Poisson	0.15	0.20	0.15	0.20	0.15	0.15	0.20	0.15
G_f [N mm/mm ²]	0.049	0.065	0.090	0.078	0.040	0.045	0.069	0.072
G_c [N mm/mm ²]	3.0	3.0	8.0	10.0	6.0	1.8	2.0	5.0
Smearred Crack Model	Fixed				Fixed			
Tensile Softening	Exp. ⁽¹⁾	Hordijk	Exp. ⁽¹⁾	Exp. ⁽¹⁾	Hordijk			
Compression Diagram	Parabolic				Parabolic			
Shear Retention Mode	Constant				Constant			
α Shear Retention	0.01	0.03	0.008	0.013	0.033	0.033	0.043	0.033

Table 4. Reference value of fracture energy as a function of aggregate size by CEB/FIP Model Code [34].

d_{max} [mm]	G_{F0} [N/mm]
8	0.025
16	0.030
32	0.058

The results were compared not only based on the load-displacement behavior but also regarding cracking and longitudinal reinforcement strain. These results confirm the reliability of the proposed numerical models and enable indirect observation of the shear behavior.

4 RESULTS AND DISCUSSION

4.1. Load and displacement

Figure 4 shows the variation of load with displacement for the S-Series numerical models for concrete with aggregates size ranging from 9.5 mm to 51 mm, comparing them with the reference models used by Sherwood [26].

The 9.5 mm and 19 mm models showed greater rigidity behavior at the beginning of the curve, especially in the initial linear behavior of the parameterized concrete. When the specimens began to crack, they lost their rigidity and developed a similar behavior as that of three experimental reference models, obtaining an ultimate load close to the experimental value.

This rigid behavior is even more apparent in the numerical models for specimens with 38 mm and 51 mm aggregates. However, a trend like the experimental curve was observed throughout the development of the analysis.

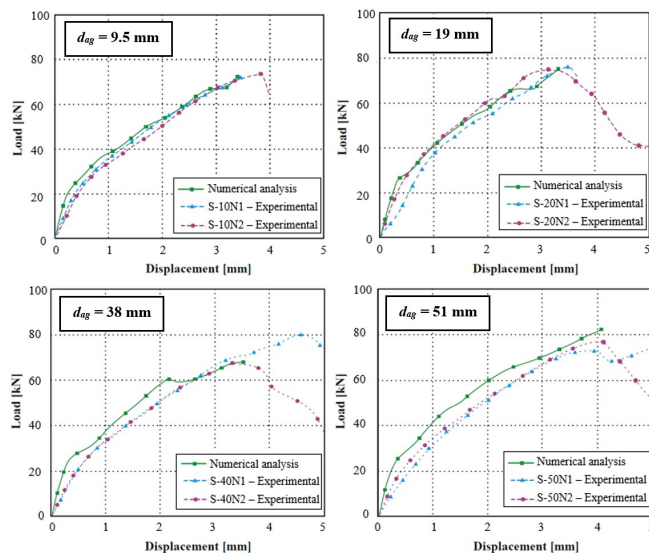


Figure 4. Load versus displacement curves for S-Series beams.

A varying load level, with a sequential increase in displacement, may lead to shear failure and the samples may become brittle like the experimental behaviors reported by Sherwood [26].

For the four numerical analyses conducted in the L-Series, the equivalence conditions between the numerical and experimental models showed similar characteristics, as shown in Figure 5. The choice of elasticity module at the beginning of loading did not show discrepancies.

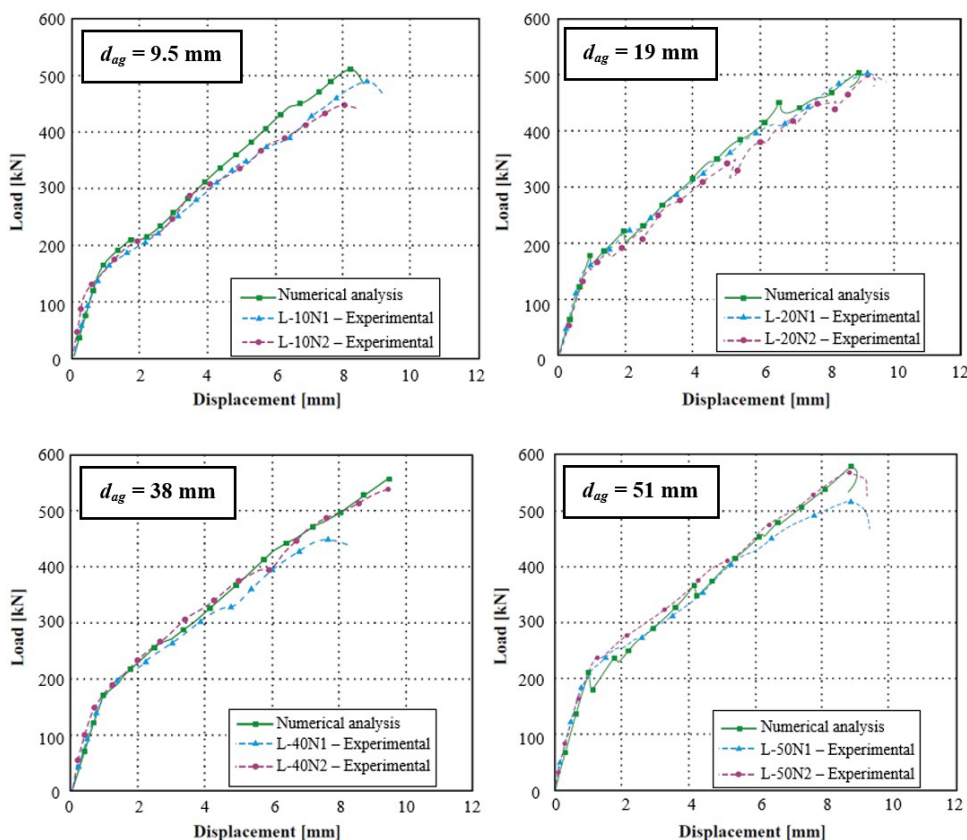


Figure 5. Load versus displacement curves for L-Series beams.

The variation between the behaviors of beams with different aggregate diameters can be understood by using the results for beams with 9.5 mm and 51 mm aggregates, which represent the two extreme aggregate sizes used in the analysis. Their concrete strengths show a difference of less than 2.0 MPa for experimental strength of concrete.

In the S-Series models, the ultimate load, ultimate displacement level, and ductility remained almost constant. The strength gain was more apparent for the L-Series, in the ultimate loads of both S and L-Series, with a difference of approximately 100 kN between the average values. The L-Series models exhibited similar stiffness and showed no major variations at the rupture.

4.2. Strains at the flexural reinforcement

The behavior of the longitudinal reinforcement of the model, referring to the axial deformations observed under the equilibrium torque of beams subjected to bending moment, can be observed for the analyzed beams, as shown in Figures 6 and 7. The values were compared with those obtained by strain gauges fixed to the reinforcements in the center of the span of the evaluated beams.

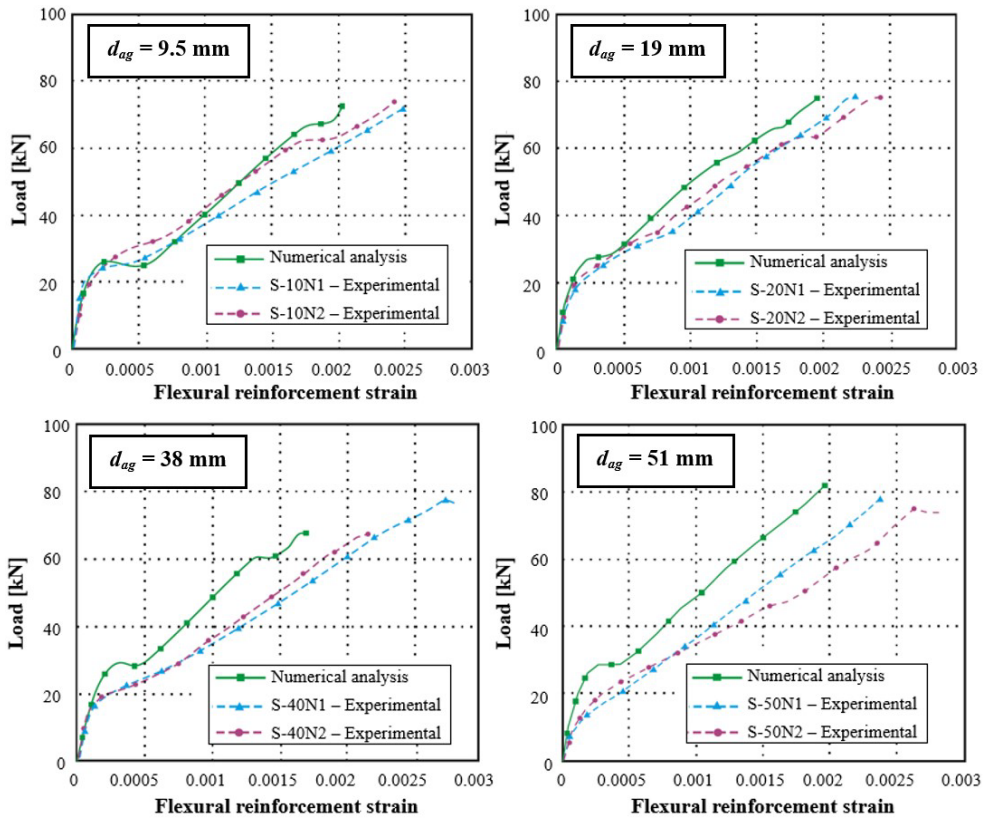


Figure 6. Load versus flexural reinforcement strain curves for S-Series beams.

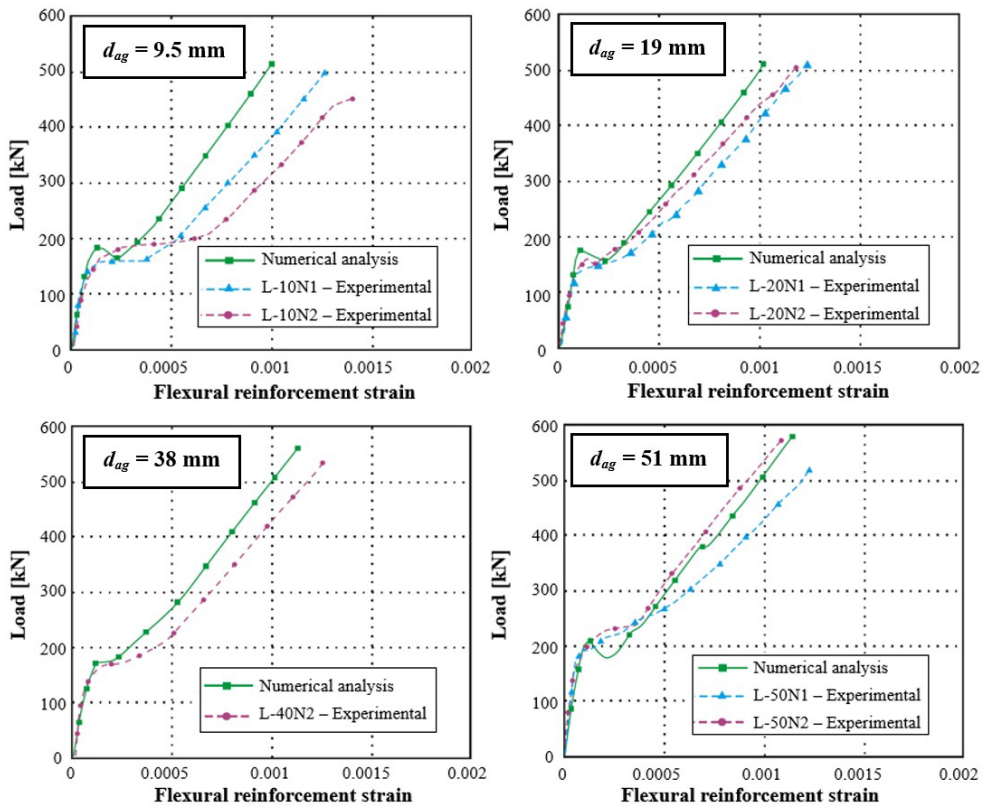


Figure 7. Load versus flexural reinforcement strain curves for L-Series beams.

The numerical and experimental comparison of the reinforcements sought to understand the deformations verified by the structural response of the model, while ensuring that no equivalence between the curves (Figures 6 and 7) by any resistant phenomena, such as bending failures, and that the ultimate shear load that occurred in the experimental tests was preserved. Based on the results, it can be noted that despite the numerical models tending to behave more rigidly than the respective experimental values, good approximations were numerically registered, indicating an effective modeling of the deformation and rupture conditions of the experimental reference model.

4.3. Cracking patterns

Figures 8 and 9 show cracking occurring in the S and L-Series beams, respectively, with their critical crack loads marked. Based on the figures below, the influence of the diameter of the aggregate can be understood by comparing the samples sized from 9.5 mm to 51 mm. The inclination of the slope gradually reduced as the nominal size of the aggregate increased for the S-Series, representing only minor changes in the L-Series cracks.

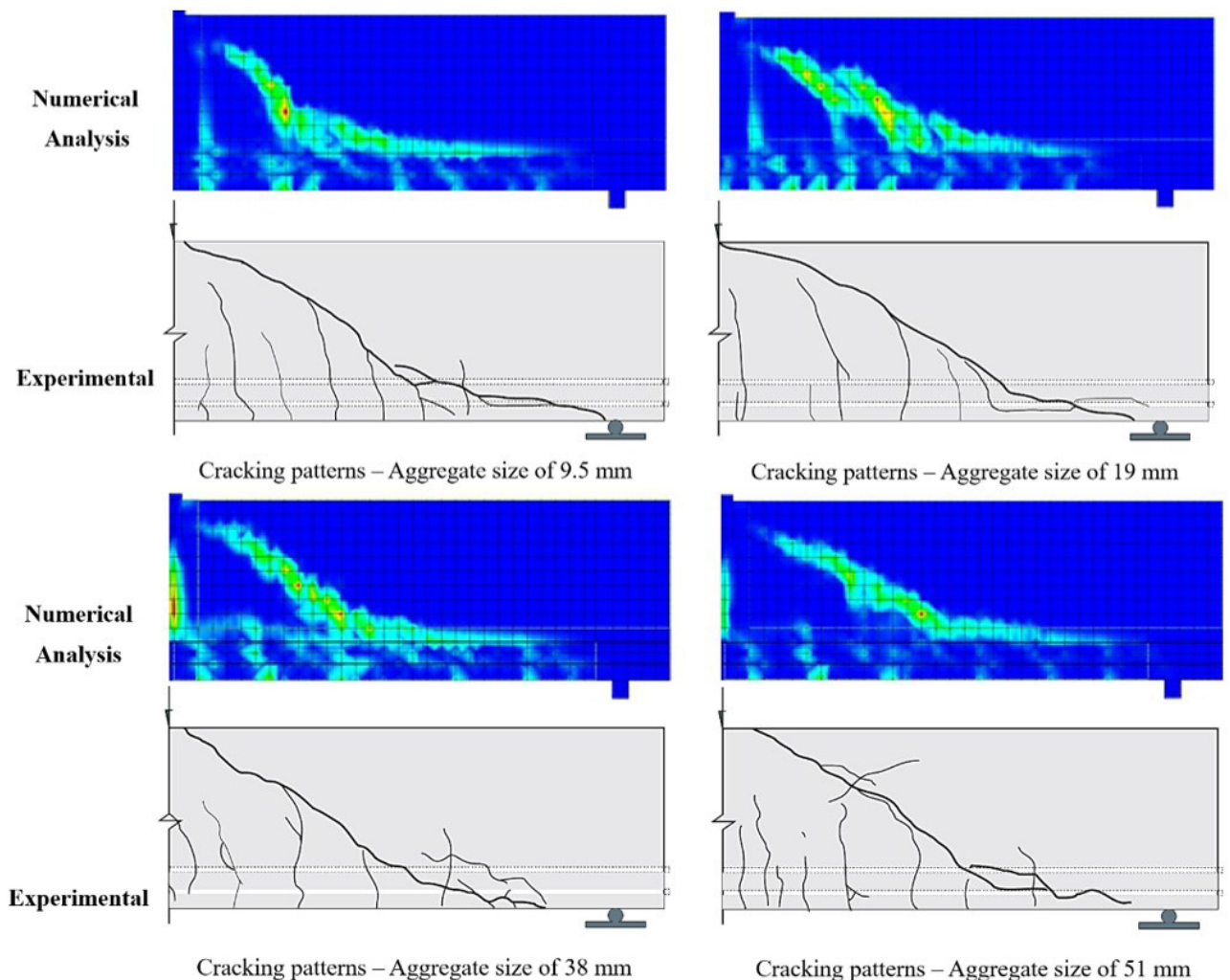


Figure 8. Numerical and experimental comparison for S-Series beams.

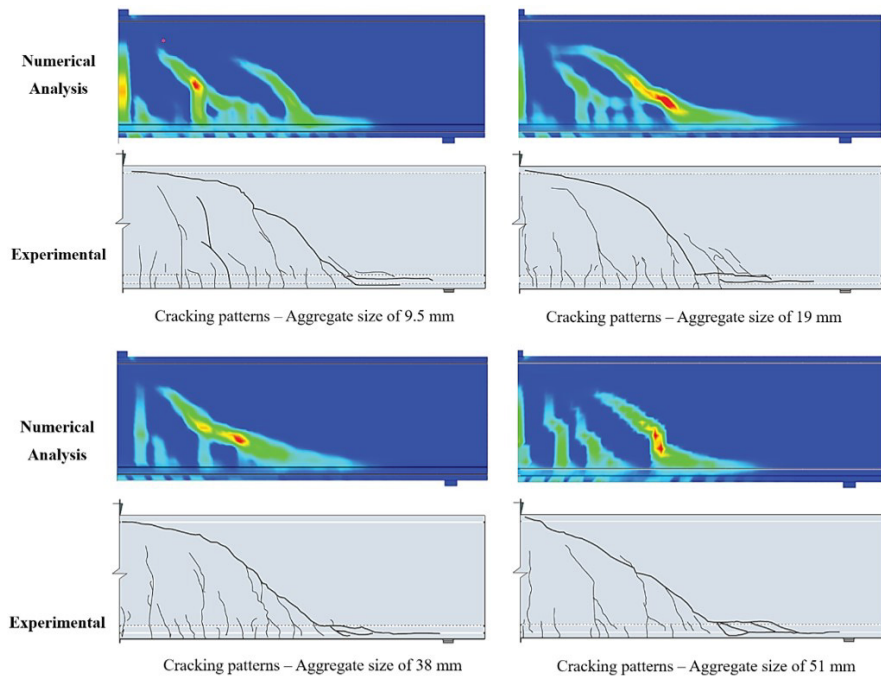


Figure 9. Numerical and experimental comparison for L-Series beams.

4.4. Internal shear strength mechanisms of RC beams without stirrups

The behaviors and derivations of the shear strength plots based on the internal concrete mechanisms in the immediate moments preceding the rupture were obtained from two distinct surveys. The first survey involved identifying a compressed strip of concrete just above the critical crack, and the second involved obtaining the shear force acting on the longitudinal reinforcement, identified as the dowel force. Figure 10 shows the horizontal compression stresses occurring in the beam with 9.5 mm aggregates for the S and L-Series beams, alongside the shear profile distributed in the area above the crack in two reference sections, A and B.

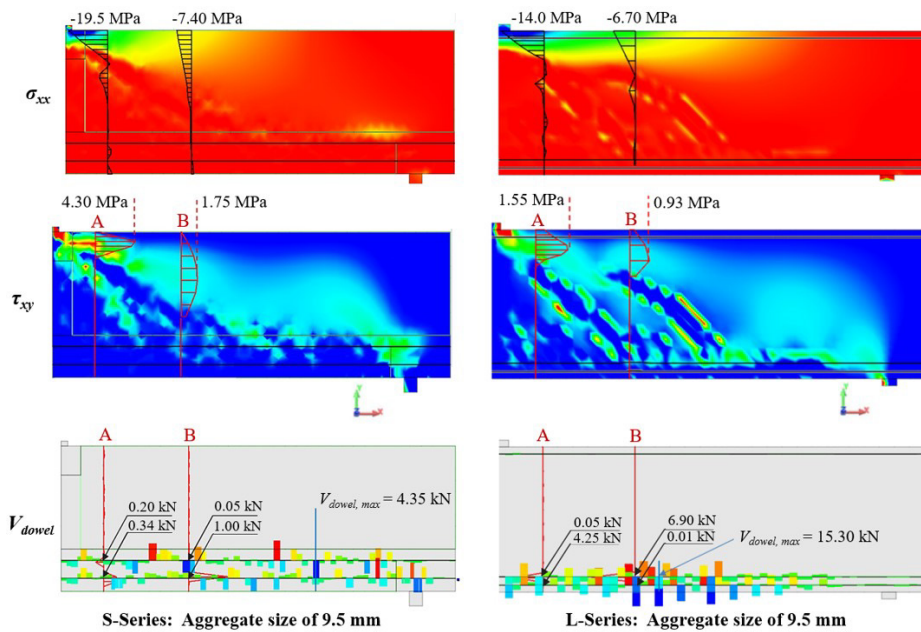


Figure 10. Compression and shear stresses and dowel effect for beams with 9.5 mm size aggregates.

Section A is in the vicinity of the load, close to the top of the critical shear crack, and section B is at a distance d from the center of the span of the beam, adopted as the authors' choice. In these studies, the chosen reference lines become relevant due to easily discriminating the influence of each of the plots at different distances from the supports, avoiding inconsistent readings on the real influence of each mechanism on the total shear force.

In the numerical analysis procedure, the steps for obtaining the shear plots were performed using the following criteria. Firstly, the intact and non-cracked regions of the compression zone above the critical crack are identified with a compression stress diagram in the horizontal direction of the stress map σ_{xx} . The end of the compressed zone is delimited using the correct coordinates of the point where the compressive stresses begin to be replaced by the tensile stresses. This premise is important since active shear stresses where the crack has occurred can also be observed from the shear distributions transferred by the beam body in the distributed crack mode. Thus, when the compression zone is properly delimited, the numerical procedure guarantees better precision and efficiency in the derivation of the shear strength plots.

Based on the distribution of shear stresses τ_{xy} obtained in sections A and B of the S and L-Series, one can conclude that the closer to the peak of the critical crack the stress is measured, the smaller is the compression zone, adding to the intensity of the shear stresses transmitted above the crack. Unlike the S-series, the larger scale beams of the L-series showed a lower shear stress intensity transferred through the compression zone, even with external loading intensities considerably higher than that of the S-Series. At points near the center of the span, the crushing stresses are also more concentrated, reaching almost 50% of the maximum concrete compressive strength (f_c). For section B, the maximum stresses are less intense, which is distributed over a larger compressed area above the crack.

Based on the analysis of Table 5, the shear force transferred by each of the complementary concrete mechanisms was quantified for the reference sections of the S- and L-series beams. In this study, the procedure consists of identifying the shear portion transferred by the compression zone V_{cz} and the dowel action V_{dowel} of the analyzed beams, and then subtracting the terms following the relation $\overline{V}_{agg} = V_{exp} - \overline{V}_{cz} - V_{dowel}$, where V_{exp} is the experimental shear force, calculating the mean contribution to the total shear force by aggregate interlock mechanism in the reference sections A and B.

Comparing the values obtained for each strength phenomenon, V_{agg} increased gradually as the maximum diameter of the aggregate in the mixture increased, as shown in the last column of Table 5, starting with $\%V_{agg}$. This behavior was also discussed by Queiroz [35] and MacGregor and Wight [36], in which they concluded that the shear force by aggregate interlock increases as the coarse aggregate increases its diameter, consequently, the rugosity of the crack surfaces also increases. In this way, a greater shear stress is transferred across the cracks.

Table 5. Plots of shear force obtained by numerical analysis of each of the internal mechanisms of resistant concrete.

Specimen	V_{exp} [kN]	Section	V_{cz} [kN]	$\%V_{cz}$ [%]	\overline{V}_{cz} [kN]	V_{dowel} [kN]	V_{agg} [kN]	$\%V_{agg}$ [%]	$\%\overline{V}_{agg}$ [%]
S-10	36.1	A	17.6	48.7	63.8	0.55	17.95	49.7	33.8
		B	28.5	78.9		1.05	6.55	18.0	
S-20	37.4	A	16.7	44.6	50.3	1.15	19.55	52.0	41.3
		B	21.0	56.1		4.85	11.50	30.7	
S-40	34.0	A	16.1	47.3	59.1	1.25	16.65	49.0	38.3
		B	24.1	70.9		0.50	9.40	27.6	
S-50	41.2	A	13.4	32.5	52.3	1.05	26.75	65.0	45.5
		B	29.7	72.1		0.75	10.75	26.1	
L-10	259.6	A	102.0	39.3	37.5	4.30	153.30	59.0	60.5
		B	92.7	35.7		6.90	160.00	62.0	
L-20	254.4	A	106.9	42.2	44.1	2.00	145.50	57.0	54.4
		B	117.5	46.2		5.42	131.50	52.0	
L-40	280.4	A	94.3	33.6	45.1	4.30	181.80	65.0	53.6
		B	159.0	56.7		2.75	118.60	42.3	
L-50	288.6	A	81.9	28.4	24.1	8.11	198.60	68.8	73.1
		B	57.1	19.8		7.90	223.60	77.5	

The results of the S-series indicated that the aggregate interlock mechanism contributed to 34-46% of the shear force capacity. The predominant mechanism of shear capacity for this series was V_{cz} . The effect of the aggregate interlock mechanism is inversely proportional to the portion of the compression zone, which gradually decreases with

an increase in the aggregate size. For the L-series, this mechanism is dominated by more than half of the total shear strength force (54-73%).

Observing the stress map σ_{xx} of the compression zone, the rupture was unrelated to the crushing of the compression zone in all the models presented since stress levels were below the strength limit of concrete in each d sample.

These results confirm the conclusions proposed by Walraven and Reinhardt [37], who found that, in addition to concrete strength, the interlocking of aggregates plays an important role in the shear strength of beams. Comparing the 9.5 mm and 38 mm aggregate models, when using concrete with a lower strength, the use of aggregates with larger diameters could guarantee similar breaking loads.

During the experiments for understanding the influence of dowel action, difficulties were found in predicting the influence of the position of the bars on shear force. In distributed crack models, the deformation caused by dowel action is distributed over the width of the finite elements, not defining a perfect cut line on the bar. Therefore, shear force peaks of different intensities occur in numerous positions along the longitudinal beam. Table 6 shows the maximum shear force obtained in other sections of the analyzed beams.

Table 6. Maximum shear forces obtained by the dowel action on the results of numerical analysis.

Specimen	V_{exp} [kN]	$V_{dowel,max}$ [kN]	$\%V_{dowel,max}$ [%]
S-10	36.1	4.35	12.0
S-20	37.4	5.50	14.7
S-40	34.0	4.70	13.8
S-50	41.2	7.45	21.9
L-10	259.6	15.30	5.9
L-20	254.4	12.20	4.8
L-40	280.4	11.70	4.2
L-50	288.6	12.90	4.5

According to the results presented, the largest numerically evaluated beams, such as those represented by the L-series, did not benefit greatly from the strength mechanism of the dowel action, whose maximum contribution to the total shear strength was only 5%.

5 COMPARISON BETWEEN EXPERIMENTAL AND PREDICTED SHEAR STRENGTH FORCE

Understanding the methodologies used in the technical standards for predicting the shear strength mechanisms of concrete is a crucial part of studying shear in reinforced concrete beams. According to the Model Code [23], CSA-A.23.3 [24], NBR 6118 [38], and ACI 318 [39], the transverse reinforcements are usually dimensioned to resist all excess shear that the internal strength mechanisms of the concrete are unable to supply, as expressed in Equation 2.

$$V_s = V_u - V_c \quad (2)$$

where V_u = total strength shear force ($V_u = V_{exp}$); V_s = shear strength force by transverse reinforcement; V_c = shear strength force through internal concrete mechanisms.

If V_c is overestimated, that is, V_c values obtained by numerical analysis is higher than the actual values in their respective experimental models, beams may lack relevant transversal reinforcements, passing excessive responsibility to concrete to resist shear.

To guarantee an analysis that fits the beam condition, the formulations contained in the design codes that estimate the shear strength of beams (as detailed in Appendix A) can be applied and verified. The numerical tests and analyses performed in reference by design standards used an L/h (beam length/height) ratio of 4.9 for the S-Series and of 5.3 for the L-Series.

The methods and limits applied in design standards are given below.

- CSA-A.23.3 [24]: calculation for beam elements with $L/h \geq 2.0$.
- NBR 6118 [38]: calculation for isostatic beam elements with $L/h \geq 2.0$ and for continuous elements with $L/h \geq 3.0$.
- ACI 318 [39]: calculation for beam elements with $L/h \geq 4.0$.

Table 7 shows the shear strength predictions for the eight beam models tested by Sherwood [26] using the complementary concrete mechanisms recommended by the studied standards. The safety coefficients specified in each standard were not considered in the analysis.

Based on the results presented in Table 7, it can be observed that all design standards presented favorable safety estimates for the S-series beams, except the Brazilian standard, which presented unfavorable results for the design. During the verification of the L-Series beams, the standards failed to predict the rupture load. The ACI 318 [39] standard presented more conservative results.

Table 7. Comparison of analytical shear strength force with experimental results.

Specimen	V_{exp} [kN]	V_{NBR} [kN]	V_{MC} [kN]	V_{CSA} [kN]	V_{ACI} [kN]	V_{exp}/V_{NBR}	V_{exp}/V_{MC}	V_{exp}/V_{CSA}	V_{exp}/V_{ACI}
S-10N1	36.6	51.9	29.5	26.0	28.8	0.70	1.24	1.41	1.27
S-10N2	38.3	51.9	28.7	25.3	28.8	0.74	1.34	1.52	1.33
S-20N1	39.1	49.7	29.3	26.0	27.8	0.79	1.33	1.50	1.41
S-20N2	38.2	48.7	29.4	26.1	27.4	0.78	1.30	1.47	1.39
S-40N1	41.8	40.7	24.9	22.2	24.0	1.03	1.68	1.88	1.74
S-40N2	34.9	40.7	28.1	25.1	24.0	0.86	1.24	1.39	1.46
S-50N1	38.5	53.2	32.2	28.7	29.3	0.72	1.19	1.34	1.31
S-50N2	40.6	53.2	31.1	27.7	29.3	0.76	1.30	1.46	1.39
L-10N1	265.0	602.3	243.6	208.3	191.7	0.44	1.09	1.27	1.38
L-10N2	242.0	623.1	262.0	224.1	196.6	0.39	0.92	1.08	1.23
L-20N1	265.0	526.7	265.2	229.6	173.4	0.50	1.00	1.15	1.53
L-20N2	266.0	546.7	272.3	235.8	178.3	0.49	0.98	1.13	1.49
L-40N1	242.0	489.1	288.8	252.8	164.0	0.49	0.84	0.96	1.48
L-40N2	288.0	493.8	264.6	231.6	165.2	0.58	1.09	1.24	1.74
L-50N1	272.0	629.2	327.9	287.0	198.1	0.43	0.83	0.95	1.37
L-50N2	298.0	620.0	307.8	269.4	195.9	0.48	0.97	1.11	1.52
Average						0.64	1.15	1.30	1.44
CV (%)						29.0	19.6	18.6	10.1

Assessing the accuracy of the studied standards in predicting the experimental shear force V_{exp} , Model Code [23] and CSA A.23.3 [24] proved the most capable in predicting rupture by the internal mechanisms of concrete. Model Code [23] presented the smallest variations, with a mean safety factor of 1.15 and a 19.6% variation coefficient.

For Model Code [23] and CSA A.23.3 [24], the importance of the influence of the aggregate diameter for the prediction of rupture by shear force can be inferred since they are based on MCFT.

Although NBR 6118 [38] showed fewer conservative results in the prediction of rupture for L-series beams, effective safety estimates were obtained for the S-series beams – those with a size range commonly used in most buildings – provided that all the recommended procedures and safety coefficients are applied.

6 CONCLUSIONS

Eight experimental RC beams without stirrups, separated into two series of different sizes, aggregate diameters, and compressive strength of the concrete, were studied by nonlinear numerical analysis using the DIANA software to understand the influences and contributions of the internal mechanisms of concrete on shear strength. The experimental results were compared with the estimates predicted by standards such as the Model Code [23], CSA-A.23.3 [24], NBR 6118 [38], and ACI 318 [39], to understand the ability of these codes in predicting the shear strength of beams by internal concrete mechanisms.

The nonlinear calculation method chosen in this study provided a satisfactory representation of the shearing behavior of the experimental models, showing good numerical-experimental approximations between the cracks pattern, ultimate load, strain in the longitudinal reinforcement, and the development of the deflection observed on the beam. It was concluded that the aggregate interlock phenomenon could be seen as the main form of failure for all the evaluated beams. This is due to the range of longitudinal stresses measured in the compression zone being unable to recognize the phenomenon of concrete crushing at the failure. Moreover, studying the rupture via the dowel effect of the reinforcement, which presented shear forces lower than a possible rupture, was impossible.

The outcomes suggest that, for a good approximation between the models studied, the G_f values, initially adopted according to CEB/FIP Model Code [34], must range from 100% to 70% of the total value for the S-Series beams and from 100% to 60% of the total value for L-Series. Thus, the S10 model was 70%, the S20 model 85%, and the S40 model 73%.

For both S and L-Series, the percentages of influence of the aggregate interlock mechanism gradually increased as the diameter of the coarse aggregate of the mixture increased. Comparing the 9.5 mm and 51 mm extremes with the same characteristic strengths, an increase in the capacity of the model is evidenced. The strength force increased approximately by 10 kN in the S-Series samples and by 100 kN in the L-Series samples.

Based on the normative estimates, it is concluded that in the methodologies that incorporate the influence of the aggregate diameter on the shear strength in their design equations produced better predictions on the behavior of concrete without shear reinforcement, with less than 20% of variation from the comparative numerical-experimental model.

The results of the numerical tests, as well as in the experimental test carried out by Sheerwood [26], aimed to obtain a type of brittle failure in the beams that occurs by the formation of a typical critical crack. In the numerical model, some characteristics were verified to define this type of failure, such as: longitudinal reinforcement did not present high stress or close to the yield stress (eliminating the hypothesis of failure by bending); the compressed zone presented stresses, in any direction, always at levels significantly lower than the concrete strength; and the pattern of crack formation showed a typical typology of critical shear cracking.

Note that, the rupture moment was also assumed in the experimental tests by Sherwood [26] and showed correspondence with the numerical models, resulting in even more certainty about the model's rupture moment.

7 REFERENCES

- [1] W. Ritter and H. Die Bauweise, "Construction techniques of hennelique," *Schweiz. Bauzeitung Zurich*, vol. 33, no. 7, pp. 59–61, 1899.
- [2] E. Mörsch, *Der Eisenbetonbau, seine Theorie und Anwendung*, 1st ed. Stuttgart: Konrad Wittwer, 1908.
- [3] ASCE-ACI Committee 445, "Recent approaches to shear design of structural concrete," *J. Struct. Eng.*, vol. 124, no. 5, pp. 1375–1417, 1998.
- [4] S. Campana, M. Fernández Ruiz, A. Anastasi, and A. Muttoni, "Analysis of shear transfer actions on one-way RC members based on measured cracking pattern and failure kinematics," *Mag. Concr. Res.*, vol. 35, no. 6, pp. 386–404, 2013, <http://dx.doi.org/10.1680/mac.12.00142>.
- [5] S. D. Poli, P. G. Gambarova, and C. Karakoç, "Aggregate interlock role in R.C. Thin-webbed beams in shear," *J. Struct. Eng.*, vol. 113, no. 1, pp. 1–19, 1987.
- [6] M. Fernández Ruiz, A. Muttoni, and J. Segaseta, "Shear strength of concrete members without transverse reinforcement: a mechanical approach to consistently account for size and strain effects," *Eng. Struct.*, vol. 99, pp. 360–372, 2015.
- [7] T. Paulay and P. J. Loaber, *Shear Transfer by Aggregate Interlock* (Special Publication SP-42: Shear in Reinforced Concrete 1). Detroit: Am. Concr. Inst., pp. 1–16, 1990.
- [8] H. J. P. Taylor, *Investigation of the Forces Carried Across Cracks in Reinforced Concrete Beams in Shear by Interlock of Aggregate* (Technical Reports). London: Cement and Concrete Association, 1970, pp. 42–77.
- [9] J. C. Walraven, "Fundamental analysis of aggregate interlock," *J. Struct. Div.*, vol. 107, no. 11, pp. 2245–2270, 1981.
- [10] P. D. Zararis, "Aggregate interlock and steel shear forces in the analysis of RC membrane elements," *ACI Struct. J.*, vol. 94, no. 2, pp. 159–170, 1997.
- [11] P. S. Chana, "Investigation of the mechanism of shear failure of reinforced concrete beams," *Mag. Concr. Res.*, vol. 39, no. 141, pp. 196–204, Dec 1987.
- [12] I. Jelic, M. N. Pavlovic, and M. D. Kostovos, "A study of dowel action in reinforced concrete beams," *Mag. Concr. Res.*, vol. 39, no. 141, pp. 196–204, 1999, <http://dx.doi.org/10.1680/mac.1987.39.141.196>.
- [13] E. O. L. Lantsoght, C. van der Veen, J. C. Walraven, and A. De Boer, "Case study on aggregate interlock capacity for the shear assessment of cracked reinforced-concrete bridge cross sections," *J. Bridge Eng.*, vol. 21, no. 5, pp. 2016, 2016.
- [14] T. Paulay, R. Park, and M. H. Philips, *Horizontal Construction Joints in Cast-in-Place Reinforced Concrete* (Special Publication SP-42: Shear in Reinforced Concrete 2). Detroit: Am. Concr. Inst., pp. 599–616, 1974.
- [15] H. J. P. Taylor, *Investigation of the Dowel Shear Forces Carried by the Tensile Steel in RC Beams* (Technical Report TRA). London: Cement and Concrete Association, 1969.
- [16] A. K. Tureyen and R. J. Frosch, "Concrete shear strength: another perspective," *ACI Struct. J.*, vol. 100, no. 5, pp. 609–615, 2003.
- [17] Z. P. Bazant and T. Kazemi, "Size effect on diagonal shear failure of beams without stirrups," *J. Am. Concr. Inst.*, vol. 89, no. 3, pp. 268–276, 1991.
- [18] G. N. J. Kani, "Basic facts concerning shear failure," *J. Am. Concr. Inst.*, vol. 63, no. 6, pp. 128–147, 1966.

- [19] H. P. J. Taylor, *The Fundamental Behavior of Reinforced Concrete Beams in Bending And Shear* (Special Publication 42). Detroit: Am. Concr. Inst., pp. 43–77, 1974.
- [20] F. J. Vecchio and M. P. Collins, "The modified compression-field theory for reinforced concrete elements subjected to shear," *ACI Struct. J.*, vol. 83, no. 2, pp. 219–231, 1986.
- [21] E. C. Bentz, F. J. Vecchio, and M. P. Collins, "Simplified modified compression field theory for calculating shear strength of reinforced concrete elements," *ACI Struct. J.*, vol. 103, no. 4, pp. 614–624, 2006.
- [22] A. Muttoni and M. Fernández Ruiz, "Shear capacity of members without transverse reinforcement as function of critical shear crack width," *ACI Struct. J.*, vol. 105, no. 2, pp. 163–172, 2008.
- [23] Comité Euro-International du Béton, *Fib Model Code Design Code 2010: Final Draft* (Bulletin d'Information). Lusanne: CEB, 2010.
- [24] Canadian Standard Association, *Design of Concrete Structures for Buildings*, CSA-A23.3-14, 2014.
- [25] J. C. Walraven, *Aggregate Interlock: A Theoretical and Experimental Analysis*. Delft: Delft Univ. Press, 1980.
- [26] E. G. Sherwood, "One-way shear behaviour of large, lightly-reinforced concrete beams and slabs," Ph.D. dissertation, Univ. Toronto, Toronto, 2008.
- [27] D. Daluga, K. McCain, M. Murray, and S. Pujol, "Effect of geometric scaling on shear strength of reinforced concrete beams without stirrups," *ACI Struct. J.*, vol. 115, pp. 5–14, 2018.
- [28] K. H. Yang and A. F. Ashour, "Aggregate interlock in lightweight concrete continuous deep beams," *Eng Struct. J.*, vol. 33, no. 1, pp. 136–145, 2011.
- [29] A. Belbachir, S.-Y. Alam, M. Matallah, and A. Loukili, "Size effect on the contribution of the aggregate interlock mechanism in reinforced concrete beams without shear reinforcement," *Eur. J. Environ. Civ. Eng.*, vol. 24, no. 9, pp. 1363–1380, 2020.
- [30] P. H. Feenstra, R. Borst, and J. G. Rots, "Numerical study on crack dilatancy I: models and stability analysis," *J. Eng. Mech.*, vol. 117, no. 4, pp. 733–753, 1991.
- [31] F. J. Vecchio and W. Shim, "Experimental and analytical reexamination of classic concrete beam tests," *J. Struct. Eng.*, vol. 130, no. 3, pp. 460–469, 2004.
- [32] M. Pimentel, P. Cachim, and J. Figueiras, "Deep-beams with indirect supports: numerical modelling and experimental assessment," *Comput. Concr.*, vol. 5, no. 2, pp. 117–134, 2008.
- [33] DIANA TNO, *DIANA Finite Element Analysis User's Manual Release 10.1*. Delft, The Netherlands, 2017.
- [34] CEB-FIP, *Bulletin d'Information 213/214 CEB-FIP Model Code 1990*. London: Thomas Telford, 1993.
- [35] F. O. Queiroz Jr., "Análise de resistência ao cisalhamento em peças de seções circulares vazadas utilizando a teoria do campo de compressão modificada," M.S. thesis, Fed. Univ. Pernambuco, Recife, 2014. [Online]. Available: <https://repositorio.ufpe.br/bitstream/123456789/10797/1/DISSERTA%C3%87%C3%83O%20Francinaldo%20Junior.pdf>
- [36] J. G. MacGregor and J. K. Wight, *Reinforced Concrete: Mechanics and Design*, 6th ed. New Jersey: Pearson Educ. Inc., 2012, 1157 p.
- [37] J. C. Walraven and H. W. Reinhardt, "Theory and experiments on the mechanical behaviour of cracks in plain and reinforced concrete subjected to shear loading," *Heron*, vol. 26, no. 1A, pp. 1–68, 1981.
- [38] Associação Brasileira de Normas Técnicas, *Design of Concrete Structures – Procedures*, NBR 6118, 2014.
- [39] American Concrete Institute, *Building Code Requirements for Structural Concrete and Commentary*, ACI 318R-19, 2019.

Author contributions: GFL, EAPL and MGM: conceptualization, writing, data curation, formal analysis, methodology, writing; LML and LCA: funding acquisition, supervision.

Editors: Samir Maghous, Guilherme Aris Parsekian.

APPENDIX A. Design Codes.

The design shear capacity attributed to the concrete can be taken by Mode Code [23] as

$$V_{MC} = V_{Rd,c} = k_v \frac{\sqrt{f_c}}{\gamma_c} z b_w \quad (A.1)$$

where γ_c is the concrete's safety coefficient, adopted as a unit value in this study, and $z = 0.9d$.

The k_v coefficient refers to the contribution of concrete to shear strength and, for Level 3 of approximation, it can be obtained by Equation A.2.

$$k_v = \begin{cases} \frac{0.4}{(1 + 1500\varepsilon_x)} \cdot \frac{1300}{(1000 + 0.7k_{dg}z)} \leq 0.15 \rightarrow \text{If } \rho_w = 0 \\ \frac{0.4}{(1 + 1500\varepsilon_x)} \rightarrow \text{If } \rho_w \geq \frac{0.08\sqrt{f_c}}{f_{yk}} \end{cases} \quad (A.2)$$

where,

$$k_{dg} = \frac{48}{16 + d_g} \geq 1.15 \quad (A.3)$$

where d_g is the aggregate diameter.

The parameter ε_x represents the longitudinal strain at the mid-depth of the member and shall be taken as

$$\varepsilon_x = \frac{\frac{M_u}{z} + V_u}{2(E_s A_s)} \quad (A.4)$$

where z is the distance between the compressed and the stretched chord of the truss model ($0.9d$); ρ_w is the transverse reinforcement ratio; M_u is the ultimate bending moment ($M_u = V_u l/4$); V_u is the ultimate shear force; E_s is the Young's modulus of the flexural reinforcement and; A_s is the longitudinal reinforcement area.

The standard CSA-A.23.3 [24] presents the verification of the shear safety condition through the product between the shear retention factor β and the root of the concrete's compressive strength ($\sqrt{f_c}$).

The capacity shear force can then be obtained by multiplying $\beta\sqrt{f_c}$ and the properties of the cross section such as width b_w and effective height to shear d_v , lessened by parameters referring to concrete mixing conditions λ , and a strength reduction factor ϕ_c .

$$V_{CSA} = V_c \phi_c \lambda \beta \sqrt{f_c} b_w d_v \quad (A.5)$$

where the effective shear height (d_v) can be taken as the highest value between $0.9d$ and $0.72h$.

The parameter s_{ze} for beams without transverse reinforcement is given by Equation A.6.

$$s_{ze} = \frac{35s_z}{15 + a_g} \geq 0.85s_z \quad (A.6)$$

where a_g is aggregate diameter, and s_z refers to the distance between the vertical stirrups of the structural element.

The strain effect factor (β) is given by Equation A.7.

$$\beta = \frac{0.4}{1 + 1500\varepsilon_x} \cdot \frac{1300}{1000 + s_{ze}} \quad (A.7)$$

where,

$$\varepsilon_x = \frac{\frac{M_u + V_u}{d_p}}{2(E_s A_s)} \quad (\text{A.8})$$

According to the standard NBR 6118 [38], the values of the shear-resistant portion by internal concrete mechanisms will vary based on the load condition to which the beams will be subjected.

Thus, considering the calculation model I of the Brazilian standard, in which the strut has an inclination of $\theta = 45^\circ$ and adopting the beam subjected to simple bending,

$$V_{NBR} = V_c = 0.6 f_{ctd} b_w d \quad (\text{A.9})$$

$$f_{ctd} = \frac{0.21}{\gamma_c} f_c^{2/3} \quad (\text{A.10})$$

where, f_c is the compressive concrete strength; b_w is the width of the element; d is the distance from extreme compression fiber to centroid of longitudinal tensile reinforcement and γ_c is the concrete's safety coefficient, adopted as a unit value in this work.

According to ACI 318 [39], the shear strength of non-prestressed members is a function of concrete strength, axial load acting on section, size effect, section area, effective depth, member width, and longitudinal reinforcement ratio. For beams without shear reinforcement (A_v), the shear strength of the concrete (V_{ACI}) is given by Equation A.11.

$$V_{ACI} = V_c = \left(0.66 \lambda_s \lambda (\rho_w)^{1/3} \sqrt{f_c} + \frac{N_u}{6A_g} \right) b_w d \quad (\text{A.11})$$

where N_u is the axial load; A_g applies to the gross cross-sectional area; ρ_w is the longitudinal reinforcement ratio of the tension reinforcement ($\rho_w = A_s/b_w d$); and λ is the factor for standard or lightweight concrete. The $N_u/6A_g$ value shall not greater than $0.05f_c$.

The size effect modification factor shall be determined by Equation A.12.

$$\lambda_s = \sqrt{\frac{2}{1 + 0.004d}} \leq 1.0 \quad (\text{A.12})$$

Additionally, the shear strength V_c is limited to the maximum value $V_{c,max}$ as

$$V_{c,max} = 0.42 \lambda \sqrt{f_c} b_w d \quad (\text{A.13})$$